Large Single-Crystal Hexagonal Boron Nitride Monolayer Domains with Controlled Morphology and Straight Merging Boundaries

*Jun Yin, Jin Yu, Xuemei Li, Jidong Li, Jianxin Zhou, Zhuhua Zhang, and Wanlin Guo**

2D hexagonal boron nitride (h-BN) has attracted intense research interest not only owing to its similarity in lattice and strength to graphene but also because of its unique properties for potential applications.[1] In contrast to semimetallic graphene, h-BN is a wide band gap insulator and could serve as an excellent dielectric with atomic-level thickness and smoothness.[2,3] Moreover, the strong ionicity of B–N bonds can localize the electronic states in h-BN and endows them with supreme thermal stability and chemical inertness.[4] These fascinating properties make the h-BN an ideal component for fabricating high performance devices by hybridizing with other 2D materials. Indeed, field effect transistors constructed with heterogeneously stacked graphene and h-BN have shown exceptionally high ON–OFF ratio and electronic mobility,[3,5] compared to those built on SiO_2.

Nevertheless, the exceptional performance is limited largely to h-BN samples obtained by mechanical cleavage method, which is difficult to scale up for real applications.[3,5] Toward large scale fabrication of devices, h-BN of large area now could be prepared by chemical vapor deposition (CVD) and cosegregation approach.[6–8] However, the limited grain size and unavoidable grain boundaries (GBs) in CVD grown h-BN always significantly impair its performance and the stability of devices. Moreover, the electronic properties of graphene are sensitive to its stacking orientation relative to the lattice of the underlying h-BN substrates.[9,10] The GBs presented in h-BN films will certainly induce localized electronic states within the band gap, which not only enhance the electronic scattering but also degrade the dielectric properties.[11]

While a number of intensive efforts have been made to grow h-BN monolayer with large grain size via CVD,[12,13] the related progress is rather limited. Tay et al. demonstrated the growth of hexagon-shaped h-BN grains with a size of 35 μm^2 on highly electropolished copper surfaces.[12] The nucleation density of h-BN grains can be reduced by increasing thermal annealing duration of the copper foil and the size of produced triangle-shaped h-BN grains can be increased to 100 μm^2.[13] Until very recently, taking Cu–Ni alloy as the substrate, the h-BN grain size can reach 7500 μm^2.[14] However, further enlarging the grain size and reducing the density of GBs ask for understanding the influence of many other factors to the growth of h-BN. Unlike graphene, the binary structure of h-BN limits the choice of the precursor, and precise control of the precursor is critical to the growth of high quality h-BN. Moreover, as the stitch of nearby domains is inevitable in the growth of continuous h-BN films, knowledge concerning the merging boundary of the h-BN domains is essential for the deep understanding of the film properties. Although there has been a good understanding on the structure and morphology of GBs in graphene, the GBs in h-BN remain rather elusive. The observation of h-BN GBs via ultrahigh-resolution transmission electron microscopy is merely at the atomic scale,[15] and large-scale information regarding the distribution of the GBs is not available yet.

Here, we demonstrate the growth of single-crystal and uniform h-BN monolayers on copper with controlled grain size and domain morphology. The single crystal h-BN sizes with respect to the nucleation density shows a notable dependence on the partial pressure of the source gas. We observe exceptional shape evolution of a single h-BN grain from triangular to hexagonal with increasing Cu vapor, allowing morphology control to achieve versatile properties. Of more interest is that the merging boundaries between the h-BN grains are composed of straight segments at the micrometer scale as being visualized by a hydrogen etching method.

In our work, ammonia borane was used as the precursor and placed in an isolated quartz container with controlled temperature as previously demonstrated.[16,17] As shown in **Figure 1**a, copper foil was wrapped into a tube with a diameter of 4 mm, and placed at the center of the quartz tube furnace with a diameter of one inch. The copper foil was first annealed at 1035 °C for 2 h with a hydrogen flow rate of 4 sccm at a pressure of 50.0 Pa. We carefully adjust the temperature of the precursor between 60 and 90 °C and keep the gas pressure at 50.4 Pa, producing an ultralow partial pressure of ≈0.4 Pa for the precursor gas. Note that the partial pressure of the precursor gas will fluctuate with increasing heating time if keeping the precursor temperature at a

J. Yin, J. Yu, X. Li, J. Li, Prof. J. Zhou, Prof. Z. Zhang, Prof. W. Guo
State Key Laboratory of Mechanics and Control of Mechanical Structures
Key Laboratory for Intelligent Nano Materials and Devices of the Ministry of Education
Institute of Nanoscience
Nanjing University of Aeronautics and Astronautics
29 Yudao Street, Nanjing 210016, China
E-mail: wlguo@nuaa.edu.cn

DOI: 10.1002/smll.201500210

www.MaterialsViews.com

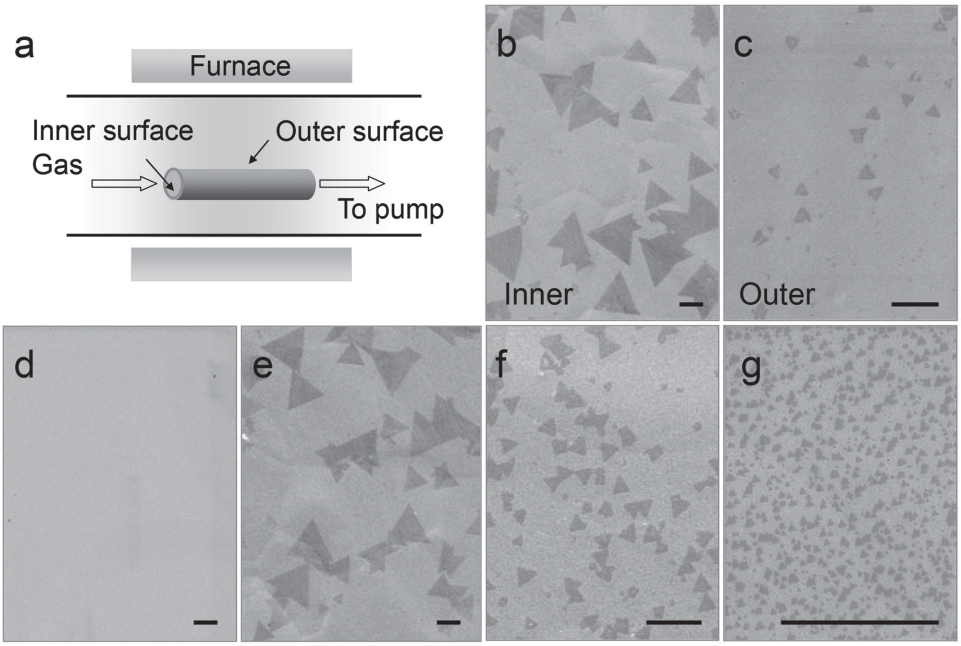

Figure 1. Growth of h-BN with large grain size. a) Configuration of the copper tube placed in the furnace. b,c) SEM images of triangle-shaped h-BN grains grown on the inner (b) and outer (c) surfaces of the Cu tube under a precursor partial pressure of 0.4 Pa. d–g) Series SEM images showing the sensitivity of the nucleation density and grain size on the inner surface of Cu tube to the precursor partial pressure, 0.1, 0.4, 1, and 3 Pa for (d), (e), (f), and (g), respectively. Scale bars: 10 μm.

specific value, which is normally adopted in synthesizing *h*-BN (Figure S1, Supporting Information).

After 1 h of the CVD growth, the sample was rapidly cooled to room temperature. As shown in Figure 1b, triangle h-BN single crystals with side length around 20 μm was found on the inner surface of the Cu tube. In contrast, the side length of the triangle grains on the outer surface is less than 4 μm. This indicates an enhanced growth rate of h-BN on the inner surface. We attribute this to the higher concentration of Cu vapor induced by the trapped evaporation of Cu,[18] which would catalyze the dissociation of the precursor gas more efficiently and thus provide more boron and nitride sources than do on the outer surface. The side length of the triangle h-BN grain found on the inner surface can reach up to ≈40 μm (Figure S2, Supporting Information).[13] With longer growth time, the h-BN grains will meet each other and merge to form a continuous film (Figure S3, Supporting Information). The large size of the single-crystal grains could greatly reduce the fluctuation of the electrical performance of the h-BN film introduced by the GBs, making it a uniform dielectric and substrate for other two dimensional materials.[13,17]

We found that the nucleation density of the h-BN grains is ultrasensitive to the partial pressure of the precursor gas. Figure 1d to 1g show series scanning electron microscopy (SEM) images of Cu foils using the same growth conditions but different precursor partial pressure of 0.1, 0.4, 1, and 3 Pa, respectively. It is clearly shown that nucleation density shows a notable dependence on the precursor partial pressure, increasing from 0 to ≈4 μm^2, with a great shrinkage of the average grain size. These results show a close correlation between the suppressed nucleation density and the ultralow partial pressure of the precursor gas.

To examine the quality of the as-fabricated h-BN film, X-ray photoemission spectroscopy (XPS) was performed on h-BN films transferred on a 300 nm SiO_2/Si substrate. As shown in **Figure 2**a, the peaks contributed to the B 1s and N 1s are both observed in the XPS spectrum, with the atomic ratio of boron to nitrogen being determined to be 1.08. Thus the as-synthesized films are dominantly composed of B–N bond and the local bonding of B and N atoms belongs to sp^2 hybridization. The layer number of the as grown h-BN films was first examined by measuring its thickness using atomic force microscopy (AFM). Figure 2b shows an AFM topography image of h-BN film with a crack introduced during the transferring process. The insert height profile across the crack edge indicates a thickness of ≈0.3 nm for the h-BN sheet, consistent with the equivalent thickness of a single-layer in bulk h-BN. The layer number was further confirmed by the transmission electron microscopy (TEM) image of the domain edge (Figure 2c). The crystalline structure of the grown h-BN domain was characterized by the selected area electron diffraction (SAED) taken at different locations as marked in Figure 2d. All the SAED patterns show clear sixfold symmetric diffraction spot, indicating well-crystalline structure of the sample. Moreover, diffraction patterns recorded at different locations show the same orientation, demonstrating that the h-BN domain is single crystal (Figure 2e–i). Note that the zigzag orientation (indicated by the red dashed line in Figure 2e) of the h-BN lattice deduced from the SAED pattern is nearly parallel to the highlighted edge of the triangles shown in Figure 2d, indicating that the edges of the h-BN domain are along the zigzag orientations, consistent with previous results.[19,20] UV–vis adsorption spectrum of an h-BN film transferred onto a transparent quartz substrate was also

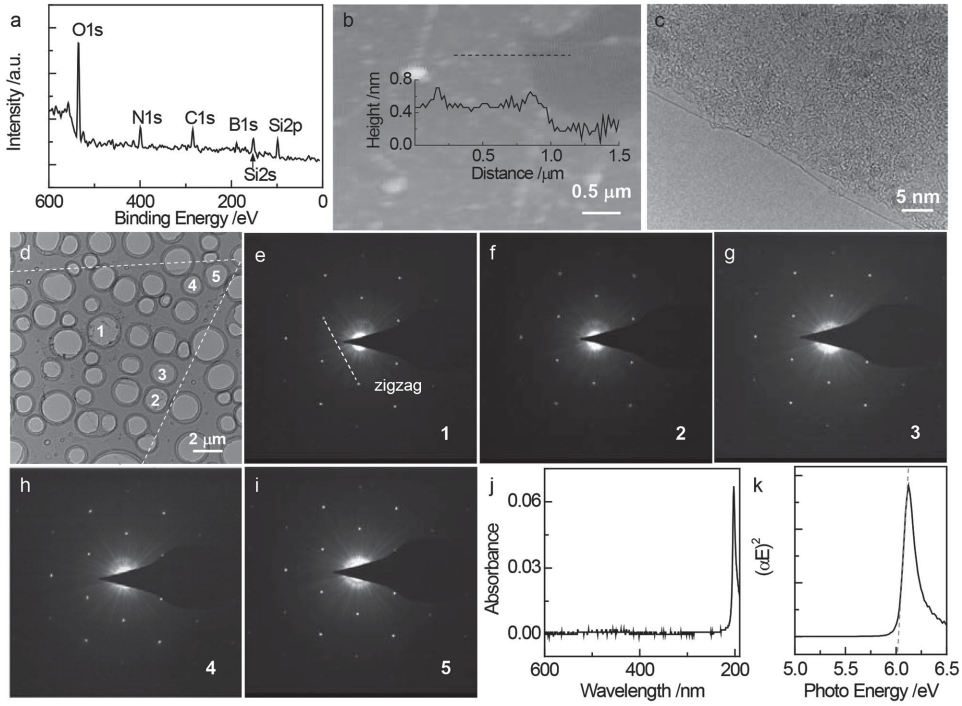

Figure 2. Characterization of the h-BN. a) XPS spectra of h-BN transferred onto a SiO_2/Si substrate. b) AFM topography image of a crack containing h-BN film on a SiO_2/Si substrate. The insert height profile across the edge indicates a thickness of the h-BN around 0.3 nm. c) High resolution TEM image of the edge of h-BN domain, indicating that it is mono-layered. d) A TEM image of a triangle h-BN domain supported on the carbon grid. e–i) SADE patterns recorded on different locations of the domain marked in (d). The red dashed line in (e) indicates a zigzag orientation of the h-BN lattice deduced from the SADE pattern. j) UV–vis absorption spectrum of the h-BN film on transparent quartz substrate. k) Plot of $(\alpha E)^2$ versus photon energy, by which the optical band gap of h-BN sheet is determined.

taken. Figure 2j shows that there is nearly no adsorption in the visible-light range but a sharp absorption peak at 202 nm, further indicating the high quality of the h-BN film. Based on the adsorption spectrum, the optical band gap of our h-BN film is determined to be 6.01 eV according to a model for direct band gap semiconductor (Figure 2k).[8] This value is very close to previous theoretical and experimental values for monolayer h-BN but slightly higher than that of bulk h-BN (5.2–5.4 eV).[21]

It has been shown that the concentration of Cu vapor has a major impact on the growth of h-BN. To further investigate the role of Cu vapor, we bended a 1×3 cm Cu foil and crimped the two contact sides to make a Cu pocket with two opened ends placed perpendicular to the gas flow direction, as illustrated in **Figure 3**a. As the spacing between the top and bottom sides decreases significantly from the bending end to the crimping end, there should be a concentration gradient of Cu vapor along this direction, with a near equilibrium vapor pressure at the crimping end and a reduced partial pressure at the bending end due to the exchange with the carrier gas. The vapor pressure of Cu in equilibrium was reported to be around 1.42×10^{-4} Torr under the growing temperature,[22] which is considerably high and comparable to the precursor partial pressure we used. It is surprising that both the shape and grain size of the h-BN grains show a strong dependence on the locations of nucleation, as shown in Figure 3b–d for h-BN grains observed at locations marked in Figure 3a. The insets show the magnified images of the typical grains grown at corresponding locations. Here the sample was heated in air at 200 °C for 1 min, and the h-BN grains is distinctly visible by optical microscopy due to the oxidization of the naked copper surface.[13] It can be seen that the triangle are truncated more significantly as Cu-vapor concentration increases, and the shape of the h-BN grains finally evolve into a hexagon, along with the reduction in area from ≈170 to ≈60 μm^2.

It is well known that the triangular h-BN grains are prone to N-terminated zigzag edges (ZN) for their lower edge energy than that of the boron-terminated ones under a wide range of boron chemical potential.[19,20] This is consistent with the SADE results that the edges of the triangles grains direct along the zigzag orientation. Thus, the truncated triangle presented here indicates the presence of alternating N- and B-terminated zigzag edges (ZB). Tay et al. attributed the growth of hexagonal h-BN to the abundance of surface oxygen on the Cu surface.[12] However, this factor is eliminated in our case, in light of that both the triangular and hexagonal h-BN grains can grow on the same piece of Cu, which suggests the same amount of oxygen. The carrier gas should also be same for different position, thus denying it as the possible origin, which was reported by Wang et al.[23] Since other growth conditions, such as temperature, gas pressure, and substrate, remain also the same, we infer that it is the enhanced concentration of Cu vapor that results in the evaluation of the grain shape.

Although the exact mechanism of the modulation of the grain shape is still not clear, the collisions of Cu atoms in the vapor with precursor molecules in the carrier gas and with the Cu surface and the edge of h-BN flakes may play a

www.MaterialsViews.com

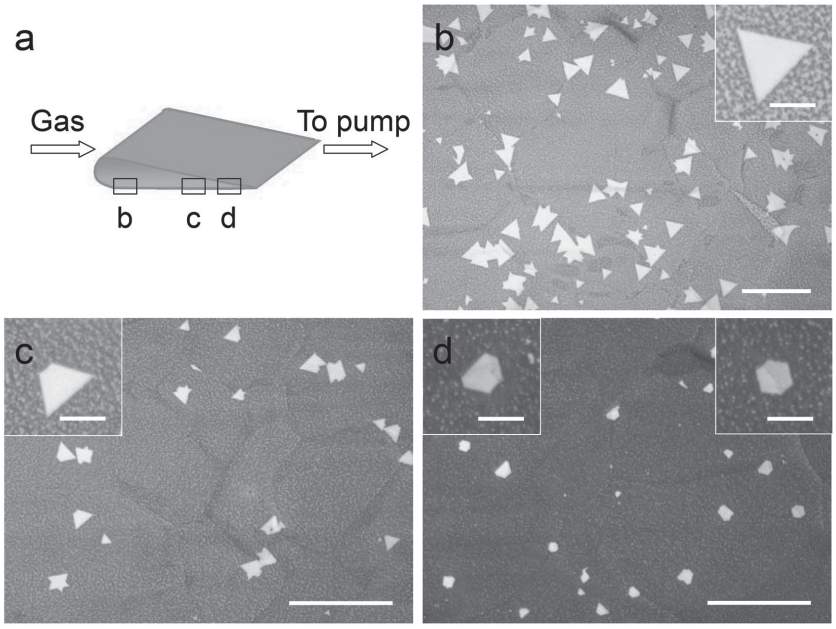

Figure 3. Modulation of the domain morphology from triangle to hexagon. a) Configuration of the Cu pocket used in the experiment. b–e) Optical image of h-BN grains at different locations marked in (a), insets showing the typical shape of the grains at the corresponding region. Scale bar: 50 and 10 μm for insets.

role. Theoretical analyses of the edge energy of h-BN have shown that both the edge energies of ZN and ZB depend notably on the chemical potential difference between B and N atoms,[24] which is in turn sensitive to the growth condition. However, the change in the edge energies should not be the only reason, as the observed grain shape cannot be predicted according to the Wulff construction.[24] Other factors, such as the kinetic energy barrier, may also be charged for the variation of the copper vapor concentration, and play an important role in the growth of h-BN. Actually, hexagonal defects with alternating ZN and ZB induced by electron irradiation have also been previously observed in the top layer of multilayer h-BN,[25] indicating that the alternating ZN and ZB edges are commonly seen in h-BN.

In addition to separated single-crystal domains, polycrystalline aggregates with stitched boundaries are also produced in the CVD growth. To reveal the merging boundaries of these polycrystalline aggregates, we cut off the precursor at the end of the growth process for 1 min, which would efficiently etch the boundaries stitching the grains. To reveal the mechanism underlying the etching of GBs in h-BN, we performed density functional theory calculations to study the adsorption of hydrogen atoms on an h-BN sheet with GBs. According to recent experiment and theory,[11,15] N-rich GBs composed of pentagon/heptagon dislocations with homoelemental N–N bonds are considered here and simulated in a ribbon model (Figure S4, Supporting Information, for the simulation models).[15] We compare the adsorption energies (E_{ad}) of a hydrogen atom on each boron and nitrogen atoms at different positions (labeled in **Figure 4**a) with respect to the GB. First, the hydrogen adsorption on the B atom is found always much more favorable than the N atom, in good agreement with previous calculations.[26] Therefore, we only take the B atom as the preferred adsorption sites in the following discussion. The energy profile of hydrogen adsorption energy on different sites across the GB is shown in Figure 4b. The adsorption energy generally increases as the adsorption site becomes closer to the GB and reaches a peak at the intermediate vicinity of the GBs. This result clearly proves that the GB is more active upon hydrogen etching. The hydrogen adsorbed at the GBs is chemically bonded to the boron atom and lift the boron out of the h-BN plane (Figure S5a, Supporting Information). The π bonds associated with the H-adsorbed boron are thus locally broken, and the neighboring N atoms become radical sites for further hydrogen adsorption. The full H chemisorptions along the GBs renders them a structural weakness to further hydrogen attack, in particular for those homoelemental bonds. As a result, a structural disruption will preferentially take place along the GB. In addition to the GB, the edges also exhibit similar chemical activity to hydrogen adsorption (Figure S5b, Supporting Information), and provide extra sites to maintain the hydrogen etching. The preferred etching at edges agrees with recent experimental reports and

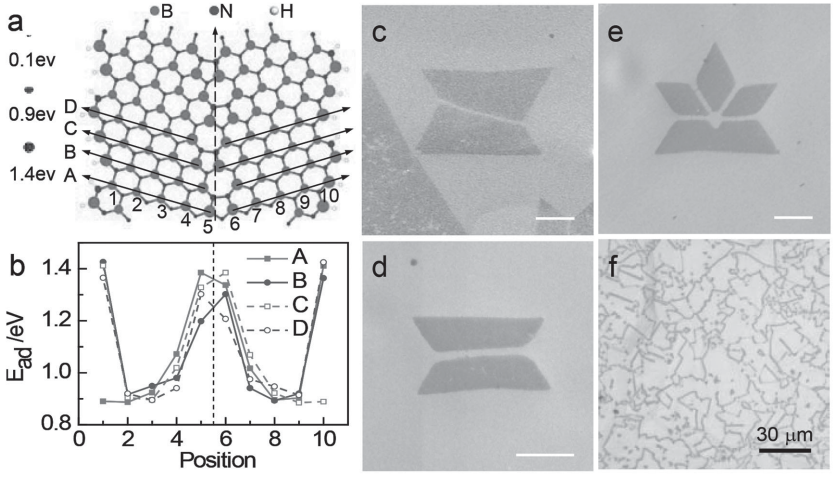

Figure 4. Merging boundaries of h-BN domains. a) The model structure with an h-BN boundary. The sizes of the boron and nitrogen atom spheres in the model represent the magnitude of the adsorption energy (E_{ad}) of a hydrogen atom on top of corresponding boron and nitrogen atoms, as labeled in the left of the figure. b) E_{ad} of boron atoms divided in groups A, B, C, and D, as marked in (a). c–e) SEM images of polycrystalline grains with etched grain boundaries. Scale bare: 5 μm. f) Optical image of large area h-BN film with etched grain boundaries.

is conformed in the following experimental results that the unzipped GBs in the h-BN monolayers already evolve into two far-separated h-BN edges (Figure 4c–f).[27]

Figure 4c shows two oppositely orientated triangles intersecting with an angle around 30° between the boundary and the parallel edges, introducing an etched straight boundary basically following the armchair direction on the micrometer scale. In addition to the tilt boundaries, we also observed the mirror twin boundary as shown in Figure 4d. Here, two truncated triangles are oppositely orientated, resulting in two isosceles trapezoids with a shared edge. Since the GBs are parallel to the edge of the triangles, it should be along the zigzag direction of h-BN at the micrometer scale. We further find that such mirror twin boundaries prevails in h-BN. In Figure 4e, we even observe for the first time an h-BN geometry of crown. Here, our etching process to the h-BN crown unambiguously demonstrates four mirror twin boundaries, all tilted at 60° (Figure 4e), which support that the crown results from an isotropic growth of multinucleus. Besides crown, stars with 6, 8, and 12 points are also observed (Figure S6, Supporting Information), embodying much richer physics in growing h-BN than growing graphene.

The hydrogen etching of GBs provides a cost-effective way to reveal the merging boundaries of h-BN film even in large area. By exposing the continuous h-BN film to hydrogen gas, the GBs of the entire film can be etched and then visible by optical microscopy with the aforementioned post air-annealing treatment. It can be seen that nearly all the GBs in h-BN tend to be strongly faceted and consist of straight lines at least on the micrometer scale (Figure 4f), in sharp contrast to the widely observed wiggly-shaped GBs in graphene. These faceted boundaries of h-BN should benefit from their corresponding formation energy, which is predicted to be more orientation-dependent than do in homoelemental 2D materials.[11] Although the orientations of the GBs at the micrometer scale could be determined through this approach, their detailed atomic structures may deviate from the regular alignment of dislocations as recently predicted and remains to be further explored by more advanced techniques.[11,28] Finally, contributed to the straight merging boundaries of the h-BN, h-BN ribbons can be fabricated by etching parallel GBs, as characterized by high magnification by SEM shown in Figure S7 of the Supporting Information. The narrowest ribbon is found to be only around 11 nm. It has been proven that 1D h-BN nanoribbons are much appealing in practical applications, as they possess tunable band gap by applied external electric field or strain and are measured to be intrinsically semiconductor due to the edge dangling bonds.[29–31] This offers us another possible route to fabricate h-BN ribbons with colorful magnetic and electronic properties,[28–30] besides the unzipping of h-BN nanotubes.[32]

In summary, we report the influence of precursor supply and Cu vapor concentration to the growth of h-BN. The size of single crystal grains can be notably enhanced by reducing the partial pressure of the precursor. Enhancing the concentration of Cu vapor by reducing the spacing between Cu foils can control the morphology of the h-BN grains from a triangle to a hexagon. Moreover, the merging boundaries of h-BN grains can be directly revealed by optical microscopy upon hydrogen etching at elevated temperature. The h-BN grains are found to adapt straight merging boundaries at the micrometer scale, giving possibility to fabricate h-BN ribbons by etching parallel GBs.

Supporting Information

Supporting Information is available from the Wiley Online Library or from the author.

Acknowledgments

This work was supported by 973 program (2013CB932604, 2012CB933403), the National NSF (51472117, 91023026, 11172124, 51375240, 51002076) of China, Jiangsu Province NSF (BK20130781, BK2011722), the Research Fund of State Key Laboratory of Mechanics and Control of Mechanical Structures (0414K01), the NUAA Fundamental Research Funds (NP2015203), Research Funds for the Central Universities (NS2014006) and a Project Funded by the Priority Academic Program Development of Jiangsu Higher Education Institutions.

[1] D. Golberg, Y. Bando, Y. Huang, T. Terao, M. Mitome, C. Tang, C. Zhi, *ACS Nano* **2010**, *4*, 2979.
[2] K. Watanabe, T. Taniguchi, H. Kanda, *Nat. Mater.* **2004**, *3*, 404.
[3] C. R. Dean, A. F. Young, I. Meric, C. Lee, L. Wang, S. Sorgenfrei, K. Watanabe, T. Taniguchi, P. Kim, K. L. Shepard, J. Hone, *Nat. Nanotechnol.* **2010**, *5*, 722.
[4] L. Li, J. Cervenka, K. Watanabe, T. Taniguchi, Y. Chen, *ACS Nano* **2014**, *8*, 1457.
[5] L. Britnell, R. V. Gorbachev, R. Jalil, B. D. Belle, F. Schedin, A. Mishchenko, T. Georgiou, M. I. Katsnelson, L. Eaves, S. V. Morozov, N. M. R. Peres, J. Leist, A. K. Geim, K. S. Novoselov, L. A. Ponomarenko, *Science* **2012**, *335*, 947.
[6] C. Zhang, L. Fu, S. Zhao, Y. Zhou, H. Peng, Z. Liu, *Adv. Mater.* **2014**, *26*, 1776.
[7] Y. Gao, W. Ren, T. Ma, Z. Liu, Y. Zhang, W. Liu, L. Ma, X. Ma, H. Cheng, *ACS Nano* **2013**, *7*, 5199.
[8] K. K. Kim, A. Hsu, X. Jia, S. M. Kim, Y. Shi, M. Dresselhaus, T. Palacios, J. Kong, *ACS Nano* **2012**, *6*, 8583.
[9] W. Yang, G. Chen, Z. Shi, C. Liu, L. Zhang, G. Xie, M. Cheng, D. Wang, R. Yang, D. Shi, K. Watanabe, T. Taniguchi, Y. Yao, Y. Zhang, G. Zhang, *Nat. Mater.* **2013**, *12*, 792.
[10] M. Yankowitz, J. Xue, D. Cormode, J. D. Sanchez-Yamagishi, K. Watanabe, T. Taniguchi, P. Jarillo-Herrero, P. Jacquod, B. J. LeRoy, *Nat. Phys.* **2012**, *8*, 382.
[11] Y. Liu, X. Zou, B. I. Yakobson, *ACS Nano* **2012**, *6*, 7053.
[12] R. Y. Tay, M. H. Griep, G. Mallick, S. H. Tsang, R. S. Singh, T. Tumlin, E. H. T. Teo, S. P. Karna, *Nano Lett.* **2014**, *14*, 839.
[13] L. Wang, B. Wu, J. Chen, H. Liu, P. Hu, Y. Liu, *Adv. Mater.* **2014**, *26*, 1559.
[14] G. Lu, T. Wu, Q. Yuan, H. Wang, H. Wang, F. Ding, X. Xie, M. Jiang, *Nat. Commun.* **2015**, *6*, 6160.
[15] A. L. Gibb, N. Alem, J. Chen, K. J. Erickson, J. Ciston, A. Gautam, M. Linck, A. Zettl, *J. Am. Chem. Soc.* **2013**, *135*, 6758.
[16] J. Yin, X. Li, J. Zhou, W. Guo, *Nano Lett.* **2013**, *13*, 3232.
[17] X. Li, J. Yin, J. Zhou, W. Guo, *Nanotechnol.* **2014**, *25*, 105701.

[18] S. Chen, H. Ji, H. Chou, Q. Li, H. Li, J. W. Suk, R. Piner, L. Liao, W. Cai, R. S. Ruoff, *Adv. Mater.* **2013**, *25*, 2062.
[19] W. Auwarter, M. Muntwiler, J. Osterwalder, T. Greber, *Surf. Sci.* **2003**, *545*, L735.
[20] W. Auwaarter, H. U. Suter, H. Sachdev, T. Greber, *Chem. Mater.* **2004**, *16*, 343.
[21] X. Blase, A. Rubio, S. G. Louie, M. L. Cohen, *Phys. Rev. B* **1995**, *51*, 6868.
[22] R. E. Honig, D. A. Kramer, *RCA Rev.* **1969**, *30*, 285.
[23] H. Wang, X. Zhang, J. Meng, Z. Yin, X. Liu, Y. Zhao, L. Zhang, *Small* **2014**, *11*, 02468.
[24] Y. Liu, S. Bhowmick, B. I. Yakobson, *Nano Lett.* **2011**, *11*, 3113.
[25] J. H. Warner, M. H. Rummeli, A. Bachmatiuk, B. Buchner, *ACS Nano* **2010**, *4*, 1299.
[26] X. Wu, J. Yang, J. G. Hou, Q. Zhu, *J. Chem. Phys.* **2004**, *121*, 8481.
[27] P. Sutter, J. Lahiri, P. Albrecht, E. Sutter, *ACS Nano* **2011**, *5*, 7303.
[28] A. M. v. d. Zande, P. Y. Huang, D. A. Chenet, T. C. Berkelbach, Y. You, G. Lee, T. F. Heinz, D. R. Reichman, D. A. Muller, J. C. Hone. *Nat. Mater.* **2013**, *12*, 554.
[29] V. Barone, J. E. Peralta, *Nano Lett.* **2008**, *8*, 2210.
[30] Z. Zhang, W. Guo, *Phys. Rev. B* **2008**, *77*, 075403.
[31] J. Qi, X. Qian, L. Qi, J. Feng, D. Shi, J. Li, *Nano Lett.* **2012**, *12*, 1224.
[32] H. Zeng, C. Zhi, Z. Zhang, X. Wei, X. Wang, W. Guo, Y. Bando, D. Golberg, *Nano Lett.* **2010**, *10*, 5049.

Received: January 22, 2015
Revised: April 14, 2015
Published online: June 3, 2015